Science Press

REVIEW

Research Progress on Corrosion Behavior and Corrosion Mechanism of Al-Cu-Li Alloy in Sodium Chloride Solution

Zhang Peng[1,2,3],   Bao Lei[1],   Rao Sixian[1],   Wu Jinjun[2],   Li Yongbing[3],   Xiong Chengyue[3], Sun Chaoyang[4]

[1] School of Mechanical Engineering, Anhui University of Technology, Ma`anshan 243032, China; [2] China Academy of Machinery Science and Technology Group Co., Ltd, Beijing 100044, China; [3] State Key Laboratory for Advanced Forming Technology and Equipment, Beijing National Innovation Institute of Lightweight Co., Ltd, Beijing 100083, China; [4] School of Mechanical Engineering, University of Science and Technology Bejing, Beijing 10083, China

Abstract: Al-Cu-Li alloy is a critical lightweight structural material in aviation and aerospace industry, which has become one of the key materials to manufacture the large aircraft structures in China. When the aircraft is in service in humid environments such as the ocean, it is vulnerable to be eroded by corrosive halide anions, and especially under the Cl⁻ ion erosion, its surface of Al-Cu-Li alloy components is prone to pitting corrosion, intergranular corrosion and exfoliation corrosion. The local corrosion of Al-Cu-Li alloy is mainly attributed to the potential difference between the alloy phase and the alloy matrix, which leads to the formation of micro-corrosion battery in the corrosive medium. The corrosion behavior of Al-Cu-Li alloy in NaCl solution and the effect of heat treatment on the corrosion resistance of the alloy were reviewed. The effects of coarse second phase particles and aging precipitates on the corrosion properties of Al-Cu-Li alloy were analyzed. In addition, the corrosion behavior in NaCl solution of different contents and electrochemical behavior in 3.5wt% NaCl solution of typical third generation Al-Cu-Li (2A97-T3, 2A97-T6, 2060-T8 and 2099-T83) alloys and conventional high strength aluminum alloy 2024-T4 used in aviation were studied in NaCl solution. The micro-corrosion morphology, corrosion electrochemical parameters and corrosion degree of each sample were analyzed. Finally, the corrosion resistance of each sample was obtained, from strong to weak in an order of: 2A97-T3>2A97-T6>2024-T4>2060-T8>2099-T83. Finally, the corrosion mechanism of Al-Cu-Li alloy in a corrosive medium was revealed, and the anti-corrosion measures of aluminum alloys in marine environments were summarized. This reseach progress provides reference for the subsequent development of the Al-Cu-Li alloy corrosion protection process and the enhancement in the corrosion resistance of aircraft in humid environments.

Key words: Al-Cu-Li alloy; alloy phase; local corrosion; corrosion mechanism; corrosion protection

Compared with the traditional aluminum alloy, the third generation Al-Cu-Li alloy has the characteristics of low density, high specific strength, stiffness, high elastic modulus, strong weldability, good wear resistance, and damage tolerance, which can meet the needs of lightweight and durable materials in the current aviation and aerospace field. Therefore, it has attracted the attention of the military industry in recent years[1–4]. The lithium has the lowest density of 0.534 g/cm³ among metal elements in nature so far. The introduction of Li element in the aluminum alloy can improve the mechanical properties of aluminum alloy. For every 1wt% lithium

added in aluminum alloy, the overall density of the material is decreased by 3%, the elastic modulus is increased by 6%, and the specific strength is increased by 9%[5–8].

At present, the third generation Al-Cu-Li alloy has gradually replaced the 2XXX and 7XXX series high-strength aluminum alloys[5–7,9–11]. Some of the third generation typical Al-Cu-Li alloys have been successfully applied in aircraft. Compared with other high-strength aluminum alloys, the 2099 Al-Li alloy also has strong corrosion resistance and fatigue crack propagation resistance, which can be used as a fuselage structure, lower wing truss, and bottom plate beam[6, 12–13]. The

2197 Al-Li alloy as the third generation of Al-Li alloy leader, has replaced the 2124 alloy adopted in the United States F16 fuselage, bulkheads, and partitions, which improves the fatigue life of aircraft to meet the 8000 h of service life requirements and reduces maintenance cost[14]. The 2060 Al-Li alloy has superior strength and fracture toughness, which is mainly used to manufacture the aircraft thin-walled components, such as aircraft skin, and wing panel, to replace the 2024-T3 and 7075-T6 high strength alloys[15–16]. The 2196 Al-Li alloy profile assembly shows a mass reduction effect due to the manufacture of aircraft floor beams, fuselage beams, struts, and seat rails[17].

Due to the long-term service of some aircrafts in coastal areas, the important parts such as fuselages and skins made of aluminum-lithium alloys are susceptible to local corrosion, which is caused by Cl⁻ ion erosion in the environment[18–19]. Local corrosion is mainly divided into: pitting, intergranular corrosion, exfoliation corrosion[20]. Under low-level stress, the stress concentration caused by pitting corrosion is the main cause of material failure[21]. Pitting is the most dangerous form of localized corrosion because it is difficult to detect and predict[20]. Local corrosion has the characteristics of great harm, high destructiveness and unpredictability, which makes the strength of aircraft components decrease, and greatly shortens the service time of aircraft. It may seriously endanger the integrity of aircraft structure and the safe operation of aircraft[22–23]. Therefore, it is crucial to investigate the corrosion mechanism of Al-Cu-Li alloy and to summarize the existing corrosion protection process of aluminum alloys in marine environments, which can provide the theoretical guidance and the practical basis for the corrosion protection of Al-Cu-Li alloy, to enhance its service life and to ensure the safety, reliability, and economy of the aircraft.

In this study, the corrosion behavior of Al-Cu-Li alloy in NaCl solution was analyzed from two aspects: the coarse second phase particles and the aging precipitated phase. The corrosion behavior of typical third generation Al-Cu-Li alloy in NaCl solution was explored by immersion method and potentiodynamic polarization curve, which provided a reference for microstructure optimization, performance regulation and anti-corrosion process investigation of Al-Cu-Li alloy.

1 Effect of Alloy Phase on Corrosion Behavior of Al-Cu-Li Alloy

The alloy phase consists of two types. One is the coarse second phase particles formed by the impurity elements and composition segregation introduced by the Al-Cu-Li alloy during the smelting process. And the other is the precipitated phase formed during the aging process[8,24–25]. The literature shows that there is a potential difference between the alloy phase and the alloy matrix due to different chemical elements of the alloy phase. In the corrosive medium, a micro-corrosion galvanic cell is formed between the alloy phase and the alloy matrix. And the alloys with different chemical composition have different effects on the corrosion behavior of Al-Cu-Li

alloys. The coarse second phase particle has a positive potential relative to the alloy matrix. It acts as a cathode to corrode the primary battery in a corrosive medium, thereby causing localized corrosion of the surrounding alloy matrix[26–28]. The main strengthening precipitated phase of Al-Cu-Li alloy is T_1 (Al$_2$CuLi) phase. Since the chemically active Li element accounts for a relatively high proportion in the T_1 phase, the corrosion potential of the T_1 phase is more negative than that of the alloy matrix. In the corrosive medium, the T_1 phase preferentially dissolves as an anode to corrode the primary battery[29–30].

Localized corrosion has seriously affected the service life and safety of aircraft in wet environments[21–23,30]. In general, pitting and intergranular corrosion are two commonest localized corrosion forms of Al-Cu-Li alloys[21–23]. In the early stage, Kertz et al[31] reported the corrosion behavior of AF/C458 (Al-Li-Cu-Mg-Zn) alloy immersed in oxidizing chloride aqueous solution. They found that pitting corrosion is closely related to the coarse second phase particles in the alloy. And the pitting corrosion occurs at grain boundaries or sub-grain boundaries, which promotes intergranular or intergranular corrosion, while the aging precipitated phase T_1 (Al$_2$CuLi) phase is the main cause of intergranular corrosion of the alloy. Buchheit et al[32] researched the pitting and intergranular corrosion behavior of AA2090 in 3.5wt% NaCl solution. And two different types of localized corrosion mechanisms are found: sub-grain boundary corrosion and second phase particle pitting. The sub-grain boundary corrosion is attributed to the selective dissolution of the T_1 phase at the sub-grain boundary. And the occurrence of pitting is due to the formation of a tiny corrosion primary battery between the coarse second phase particles (Al-Cu-Fe) and the surrounding alloy matrix, which in turn causes the alloy matrix distributed around the second phase particles to dissolve. Then a pitting pit is eventually formed. At the same time, the continuous sub-grain boundary dissolution occurs near the pitting pit, which further verifies the influence of the coarse second phase particles and the aging precipitated phase T_1 on the corrosion resistance of Al-Cu-Li alloy.

1.1 Effect of coarse second phase on local corrosion behavior of Al-Cu-Li alloy

Al-Cu-Li alloy in the smelting process will inevitably introduce Fe, Si and other impurity elements, which are combined with Al, Mg, Mn and other elements to form coarse second phase particles[25,27–28]. The second phase particles contain a variety of particles with different elemental composition. The chemical properties of the particles are also different due to the differences in the elements contained. In addition, the microstructure geometry of the particles significantly affects the fracture toughness, fatigue resistance, damage evolution, corrosion resistance, anodic oxidation behavior, and recrystallization behavior of the deformation aluminum alloys[33]. In the scanning electron microscope observation with the relative atomic mass as the contrast, the brighter the color, the larger the relative atomic mass of the

metal elements contained in the second phase particles, the less active the chemical properties, whereas the darker the color, the smaller the relative atomic mass, the more active the chemical properties[33–34].

Fig. 1a shows the backscattered electron micrograph of AA2099-T8 alloy after mechanical polishing. The size of the second phase particles is between several microns and more than 20 μm. The bright characteristics are shown in the extrusion direction[35]. Fig. 1b shows backscattered electron micrographs of Fig. 1a with increased magnification. After adjusting the contrast of the micrographs, the black part of the aluminum matrix and two types of second phase particles alone or together can be clearly seen[35]. Since the coarse second phase particles in the Al-Cu-Li alloy have a positive potential relative to the alloy matrix in the humid environment, the micron-sized second phase particles and the surrounding alloy matrix are easy to form a corrosion primary battery, which in turn causes localized corrosion of the alloy matrix[36–40].

Balbo et al[41] studied the electrochemical corrosion behavior of Li-containing AA2198-T3 and Ag-containing AA2139-T3 alloys in sodium chloride aqueous solution of different concentrations. The AA2198 and AA2139 alloys usually corrode at the alloy matrix around the copper-rich second phase particles. The chemical properties of the Cu element are not active, so the corrosion potential of the Cu-rich second phase particles is significantly higher than that of the alloy matrix. Therefore, the Cu-rich second phase particles are the cathode and the alloy matrix is corroded as the anode of the corroded primary cell. A large number of coarse intermetallic compound particles are distributed on the surface of the mechanically polished 2A97-T3 alloy, as shown in Fig.2a[27].

The bright features are intermetallic particles with sizes between 0.23 μm and 19.8 μm. The θ (Al$_2$Cu) phase accounts for 8.4% and the coarse α phase (Al-Cu-Fe-Mn-(Si)) accounts for 91.6%. By studying the corrosion behavior of 2A97-T3 Al-Cu-Li alloy in 3.5wt% NaCl solution, it is found that the localized corrosion is related to the θ phase and the coarse α phase particles. And the discontinuous localized corrosion only exists in the Al-Cu-Fe-Mn- (Si) particles in the near-surface region of the alloy matrix. As shown in Fig. 2b, the maximum corrosion depth is about 2.8 μm. The coarse intermetallic particles are usually used as inert electrodes in the corrosive medium of NaCl solution due to the high proportion of inactive Cu and Fe elements. And the surrounding alloy matrix is corroded as the anode of the microprimary battery. Thus the corrosion pits form[28].

Ma et al[28] further analyzed the corrosion behavior of AA2099-T83 alloy and the role of two types of second phase particles in the formation and expansion of localized corrosion. It was found that high-copper Al-Cu-Mn-Fe- (Li) particles and low-copper Al-Cu-Mn-Fe-(Li) particles have different corrosion behavior when they are immersed in 3.5wt% NaCl solution for the same time, as shown in Fig. 3a. The corrosion morphology is typical of low copper second phase particles. There is a narrow gap of several hundred nanometers between the alloy matrix and the particles, indicating that the alloy matrix is dissolved around the Al-Cu-Mn-Fe-(Li) particles. As shown in Fig. 3b, the bright particles marked by the white arrows are low-copper second-phase particles. And the deposited copper-rich nanoparticles produced by the dissolution of the surrounding alloy matrix have a diameter of 30−50 nm. Fig. 4b is the typical corrosion morphology of high copper second phase particles. The gap
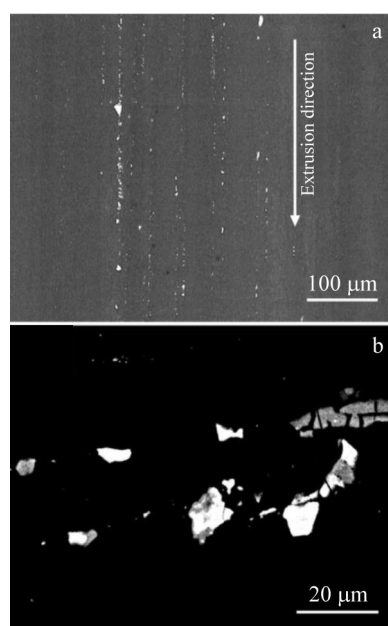

Fig.1   Distributions of second phase particles of AA2099-T8 alloy: (a) at low magnification, (b) at increased magnification[35]
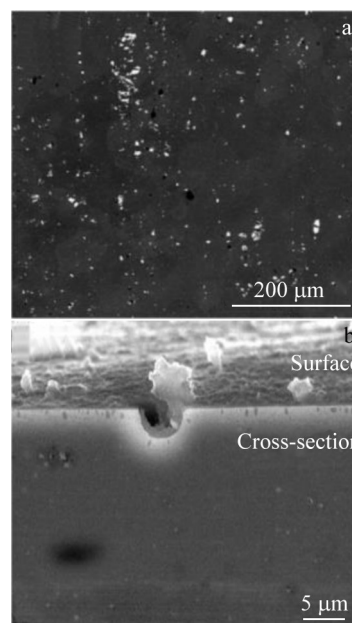

Fig.2   Morphologies of 2A97-T3 alloy: (a) mechanical polishing surface, (b) cross section of the corrosion pit after immersion in sodium chloride solution for 45 min[27]
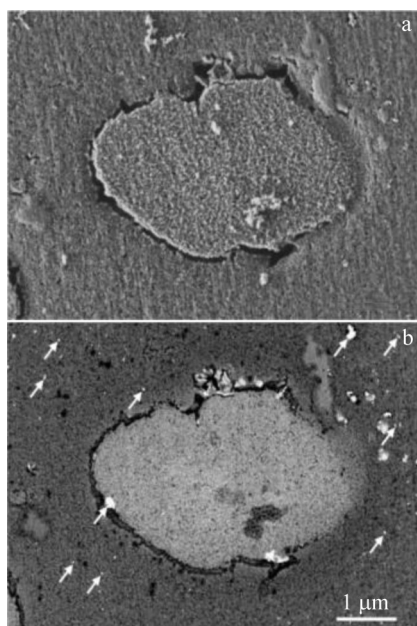
Fig.3   Morphologies of low copper content particles: (a) secondary electron image and (b) backscattered electron image[28]

between particles and the alloy matrix is relatively wide. There are obvious nanoparticles and corrosion products on the surface of residual intermetallic particles, which indicates that there is a relatively strong micro-current coupling effect between particles and the alloy matrix.

As shown in Fig. 4b, the bright feature is the residual nanoparticles formed by the preferential dissolution of Al and Li elements in high-copper Al-Cu-Mn-Fe-(Li) particles. Generally, the corrosion potential of the coarse second phase particles is higher than that of the alloy matrix due to the
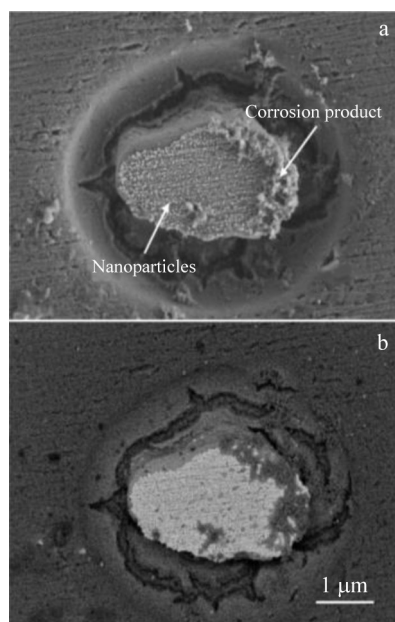

Fig.4   High copper content particles: (a) secondary electron image and (b) backscattered electron image[28]

presence of inactive elements such as Cu and Fe. However, due to the high content of Li element with active electrochemical properties in the high copper phase particles, it provides a large driving force for the selective dissolution of Al and Li elements from the high copper second phase particles, which makes it difficult to form an oxide film on the surface of the high copper phase particles, thus accelerating the local corrosion process[35,42].

In addition, the porous copper-rich residue on the dealloyed high-copper phase particles can be regarded as an efficient cathode for anodic dissolution of the surrounding alloy matrix. The specific performance is that the Al and Li elements in the high copper phase Al-Cu-Mn-Fe-(Li) particles are preferentially dissolved, resulting in self-corrosion of the high copper phase particles. And the proportion of Cu and other elements with inactive electrochemical properties increases inside the high copper phase. These Cu-rich nanoparticles then become the cathode of the galvanic cell, which further accelerates the anodic dissolution of the surrounding alloy matrix. The corrosion potential difference between the low copper Al-Cu-Mn-Fe-(Li) particles and the alloy matrix is small, so only the low copper second phase particles outside a small range of alloy matrix is corroded. And the small corrosion channels are formed along the particles around.

Due to the presence of Cu, Fe and other elements with inactive electrochemical properties and active Li elements in the coarse second phase particles in the Al-Cu-Li alloy, the coarse second phase particles have a more complex dissolution process during the corrosion process. As the corrosion process continues to deepen, the coarse second phase particles eventually evolve into residual second phase particles, which is enriched in high-potential elements such as Cu. Such residual second-phase particles will become a local corrosion source. It continues to promote the corrosion of the matrix around the coarse second-phase particles.

Lin et al[43] explored the corrosion behavior of 2099 Al-Li alloy in intergranular corrosion solution of (57g NaCl+10 mL 30% H_2O_2)/L. Fig. 5a – 5c show the TEM images of the microstructure of 2099 Al-Li alloy under the condition of under-aging. It can be seen that the precipitation strengthening phase of the alloy matrix is mainly fine δ' phase, but the δ' phase is coherent with the α (Al) matrix, which cannot affect the corrosion performance of the alloy, as shown in Fig. 5a. There are coarse residual Al-Cu-Fe-Mn particles at the grain boundaries, as shown in Fig. 5c. Due to the preferential selective dissolution of Mn with active electrochemical properties in the corrosive medium, the Al-Cu-Fe-Mn particles are transformed into residual Al-Cu-Fe-Mn particles rich in high potential elements such as Cu and Fe. The corrosion potential increases, and a corrosion micro-cell forms with the surrounding alloy matrix. It acts as an efficient cathode to promote the corrosion of the surrounding alloy matrix.

In summary, the coarse second phase particles and the alloy matrix form a miniature corrosion cell in the corrosive medium, which affects the local corrosion resistance of the
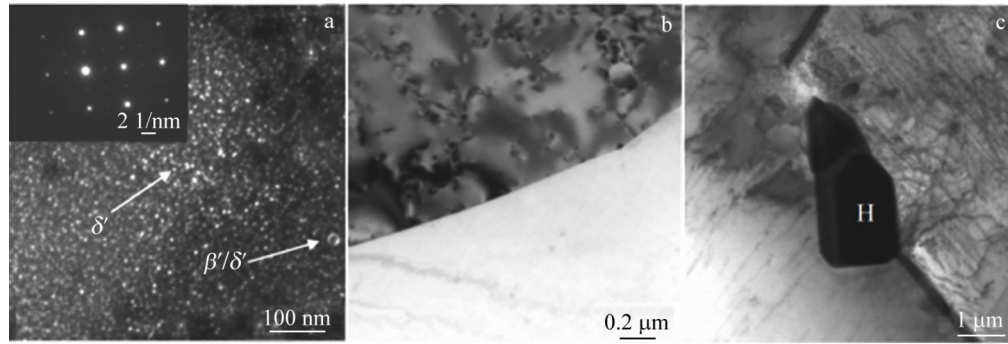
Fig.5   TEM images of 2099 Al-Li alloy under under-aging condition: (a) distribution of δ' phase, (b) grain boundary microstructure, and (c) residual Al-Cu-Fe-Mn particles at grain boundaries[43]

alloy to some extent. Ref.[44] shows that grains can be refined and distributed uniformly by means of severe plastic deformation methods such as equal channel angular pressing (ECAP), hydrostatic extrusion (HE) and torsion extrusion (ET). The effect of coarse second phase particles on the corrosion resistance of the alloy can be reduced. Nevertheless, the second phase particles after severe plastic deformation still have an adverse effect on the corrosion resistance of the alloy. In addition, severe plastic deformation treatment is mainly focused on the properties of materials such as steel, copper and nickel, while the corrosion resistance of Al-Cu-Li alloys has not been substantially researched[44].

1.2 Effect of aging precipitates on corrosion behavior of Al-Cu-Li alloy

Different from coarse second phase particles, the aging precipitates produced during aging heat treatment have a significant effect on the corrosion resistance and mechanical properties of Al-Cu-Li alloys[5-6]. The type, volume fraction and distribution of precipitated strengthening phases are also different in Al-Cu-Li alloys with different Cu/Li ratios, which affect the mechanical properties and corrosion resistance of the alloys to some extent[25]. The low Cu/Li ratio Al-Cu-Li alloy presents excellent elastic modulus, due to the large proportion of Li element in the aging precipitated phase and the $\delta'(Al_3Li)$ phase precipitated in the crystal. In high Cu/Li ratio Al-Cu-Li alloys, the T_1, T_B (Al_7Cu_4Li) and δ (AlLi) phases emerge at grain boundaries, which affect the mechanical properties and corrosion resistance of Al-Cu-Li alloys[25,27,39-40,45]. The needle-like T_1 (Al_2CuLi), disk-like θ' (Al_2Cu) and spherical δ' (Al_3Li) are the main precipitated strengthening phases of Al-Li alloy[5]. The type and distribution of alloy phases in the third generation Al-Li alloy are shown in Fig.6.

The spherical δ' phase has a LI_2 structure. It is uniform and fine in Al-Cu-Li alloy matrix, which is the main strengthening phase in the early stage of aging. There is a coherent relationship between δ' phase and α (Al) matrix. Although its potential is negative, it will not lead to local corrosion of the alloy[8,31,40]. The θ' phase has a coherent relationship with the α (Al) matrix. Due to the large proportion of the inactive Cu element in the discoid θ' phase, the θ' phase has a positive
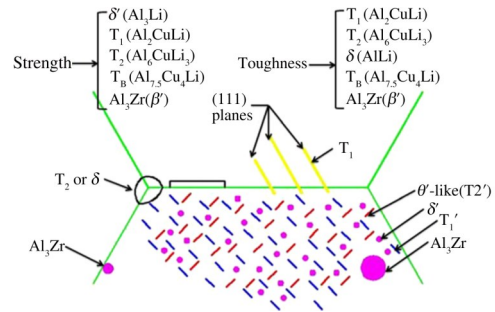

Fig.6   Types and distribution of alloy phases in the third generation Al-Li alloy[5]

potential compared to the alloy matrix. In the corrosive medium, a corrosive galvanic cell with the θ' phase is the cathode and the matrix is the anode, which causes pitting corrosion of the matrix around the θ' phase[8,46]. The T_1 phase has a space lattice of P6/mmm[35]. The lath-shaped T_1 phase is preferentially precipitated and grows at the grain boundary by consuming the intragranular δ' phase. Due to the semi-coherent relationship between the T_1 phase and the α (Al) matrix, the T_1 phase dissolves as the anode of the corroded galvanic cell during the intergranular corrosion process[8,23-24,30-31].

The corrosion potential of the aging precipitated phase depends on the constituent elements of the precipitated phase. In the aging precipitated phase, due to the active chemical properties of Li element, the aging precipitated phase containing Li element usually exhibits a lower corrosion potential. In the corrosive medium, a miniature corrosion primary battery is formed with the aging precipitated phase and the alloy matrix. And the aging precipitated phase with a high Li element content is preferentially corroded as an anode[46-47]. Rinker et al[48] studied the stress corrosion behavior of AA2020 Al-Cu-Li alloy and firstly proposed the selective dissolution mechanism of T_1 phase in Al-Cu-Li alloy. Due to the high proportion of Li element in T_1 phase, the T_1 phase exhibits active electrochemical properties. In the corrosive medium, it is easy to form a micro-corrosion primary battery with the alloy matrix. The α (Al) matrix acts as a large cathode, and the T_1 phase acts as a small anode in the primary battery to be corroded[49].

Subsequently, Buchheit et al[49] discussed the corrosion behavior of 2099-T83 Al-Cu-Li alloy in 3.5wt% NaCl corrosive medium. Due to the high electrochemical activity of the T_1 phase and the preferential dissolution of the Li element in the electrochemical reaction, the localized corrosion of the grains occurs. In addition, after the Li element in the T_1 phase is preferentially dissolved, the remaining Cu element will be re-precipitated on the surface of the T_1 phase, so that the proportion of Cu element in the residual T_1 phase increases, resulting in an increase in the corrosion potential of the T_1 phase, and finally a polarity transition occurs, forming the cathode of the corroded galvanic cell.

By studying the effect of the distribution of aging precipitates on the corrosion behavior of 2A97-T3 Al-Cu-Li alloy in 3.5wt% NaCl solution, Zhang et al[30] found that there are two needle-like precipitates with different sizes at the grain boundary. One is a long needle-like T_1 phase with a size of about 1 μm and the other is a short needle-like T_B (Al_7Cu_4Li) phase with a size of about 100 nm. The number of T_B phases distributed at the grain boundary is less. Since the T_1 phase contains a high proportion of Li element, the Li element in the T_1 phase selectively dissolves in the NaCl solution corrosion medium. The residual T_1 phase becomes a copper-rich phase, and then the corrosion potential also shifts positively. Therefore, the T_1 phase precipitated acts as the cathode of the corrosion galvanic cell to promote the anodic dissolution of the peripheral alloy matrix, resulting in the local corrosion near the high-density T_1 phase precipitates. Due to the small proportion of Li element in the T_B phase compared to that in the T_1 phase, the T_B phase exhibits relatively inert behavior in the etching test. In addition, it is also found that compared with the effect of the T_1 phase on grain boundary corrosion, the local plastic deformation at the sub-grain boundary has a more obvious effect on grain boundary corrosion propagation.

Li et al[47] investigated the corrosion mechanism of T_1 and T_2 phase precipitates in Al-Cu-Li alloys in a 3.5wt% NaCl solution. For the T_1 phase, the corrosion potential is more negative than that of $α$ (Al) at the beginning of the reaction, but the corrosion potential is more positive than that of $α$ (Al) after 10 d of immersion. For the T_2 phase, the corrosion potential is more negative than that of $α$ (Al) at the beginning of the reaction. With the extension of the soaking time, the corrosion potential of the T_2 phase is positive and then negative compared to $α$ (Al). It can be seen that the active Li element in the T_1 and T_2 phases preferentially dissolves in the initial stage of corrosion until a large amount of inactive Cu element remains in the T_1 and T_2 blocks. Since the Al element is more electrochemically active than the Cu element, the corrosion potential of the residual T_1 and T_2 phase blocks enriched with the Cu element is higher than that of the alloy matrix, which in turn causes a polarity transition in both groups of corroded primary batteries. The alloy matrix becomes an anode to be dissolved. The corrosion tendency of the T_2 phase is more serious than that of the T_1 phase due to the larger proportion of Li element and the lower proportion

of Cu element in the T_2 phase.

Based on the abovementioned results, the T_1 phase is one of the main factors affecting the corrosion resistance of Al-Cu-Li alloy. Pre-deformation of Al-Cu-Li alloy before aging cannot only release the residual stress of the alloy after quenching, but also form high density and uniform distribution of dislocations inside the alloy[50]. During the aging process after pre-deformation treatment, the high density and uniformly distributed dislocations in the Al-Cu-Li alloy provide preferential nucleation positions for the T_1 phase, which in turn promotes the uniform dispersion of the T_1 strengthened precipitates. It reduces the effect of the T_1 strengthening precipitate on the corrosion properties of the Al-Cu-Li alloy[51–53]. In addition, pre-deformation before aging promotes the precipitation of the T_1 phase in the matrix, which inhibits the formation of a non-precipitated precipitation zone at the grain boundary and which reduces the corrosion sensitivity of Al-Cu-Li alloy[54].

Li et al[55] dissected the exfoliation corrosion behavior of T6 (165 °C, 50 h) and T8 (6% pre-deformation, 165 °C, 50 h) Al-Cu-Li alloy in EXCO (4.0 mol/L NaCl+0.5 mol/L KNO_3+0.1 mol/L HNO_3, pH=0.4) solution, as shown in Fig. 7. With the same immersion time, the corrosion morphology of the T6 state sample surface is more serious than that of the T8 state sample. There are more corrosion products on the surface of the T6 alloy. The results present that the corrosion resistance of T8 alloy is better than that of T6 alloy. The distribution of T_1 phase in T6 and T8 alloys is shown in Fig.8. Due to 6% pre-deformation before aging, a large number of uniformly distributed dislocations are introduced into the T8 alloy. And the T_1 phase is preferentially precipitated at grain boundaries, sub-grain boundaries and dislocations. The T_1 phase in the T8 alloy is uniformly dispersed in the grain and at the grain
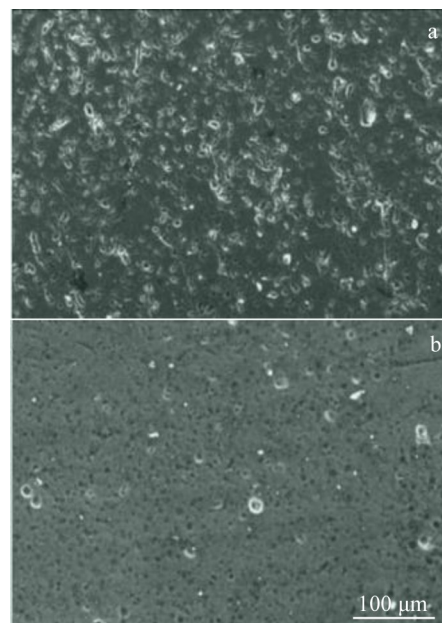

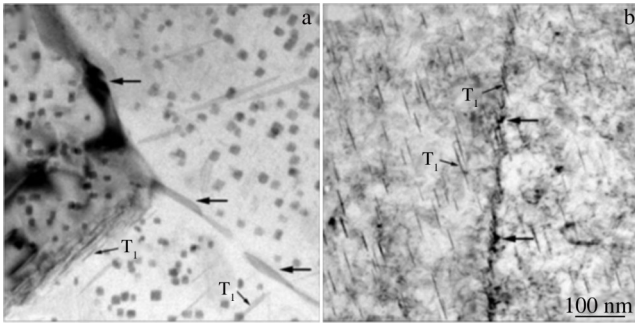Fig.7　Surface morphologies of specimens immersed in EXCO solution for 7 h: (a) T6-treated and (b) T8-treated[55]

Fig.8 Bright field TEM images of the grain boundary region of the sample: (a) T6-treated and (b) T8-treated[55]

boundary. In addition, the grain boundary equilibrium phase and the intragranular T_1 phase of the Al-Cu-Li alloy after T8 heat treatment are significantly finer than those after T6 heat treatment. Therefore, like the coarse second phase, the coarse aging precipitates are more unfavorable to the corrosion resistance of the alloy.

The results display that the pre-deformation before aging also affects the corrosion properties of Al-Cu-Li alloy. With the increase in pre-deformation, the number of dislocations in the alloy increases, which promotes the uneven precipitation of the T_1 phase at the dislocation. In addition, a large number of dislocations winding at the sub-grain boundaries provides a driving force for local corrosion of the alloy, which reduces the corrosion resistance of the Al-Cu-Li alloy[45]. Xu et al[56]

studied the effect of pre-deformation before artificial aging on the corrosion behavior of 2195 Al-Li alloy in intergranular corrosion solution (1 mol/L NaCl+10 mL 30% H_2O_2/L). As shown in Fig. 9 and Fig. 10, with the increase in pre-deformation, the intergranular corrosion degree of 2195 Al-Li alloy is more obvious, and the intergranular corrosion sensitivity of the sample increases. The cold forming with an appropriate amount of deformation is beneficial to the introduction of high density and uniformly distributed dislocations, which are prone to the uniform precipitation of aging precipitates[57]. Excessive deformation will cause dislocation entanglement in the matrix, resulting in uneven distribution of precipitated phases in the matrix. It reduces the toughness of the alloy[58].

In addition, under the same pre-deformation condition, the corrosion morphology of the alloy is more serious with the increase in aging temperature. There is a large corrosion potential difference between the T_1 phase and the grain boundary precipitate-free zone (PFZ), which forms galvanic corrosion. However, T_1 in the alloy treated by low-temperature (L-M) graded aging is less than that treated by high-temperature (H-M) graded aging. The intergranular corrosion driving force of L-M aged alloy is weak, which makes the grain boundary corrosion sensitivity of the alloy lower[56].

For heat-treatable Al-Cu-Li alloys, the aging regime improves the strength of the alloy by regulating the distribution, type and size of the aging precipitates, and also enhances the corrosion resistance of the alloy[24-45,58]. Jiang et
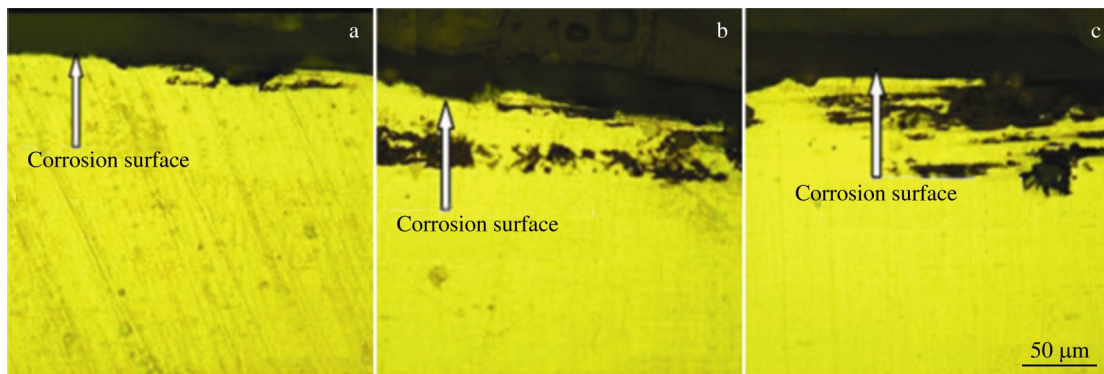

Fig.9 Morphologies of intergranular corrosion of specimens after L-M treatment with different pre-deformations[56]: (a) 3%, (b) 6%, and (c) 8%
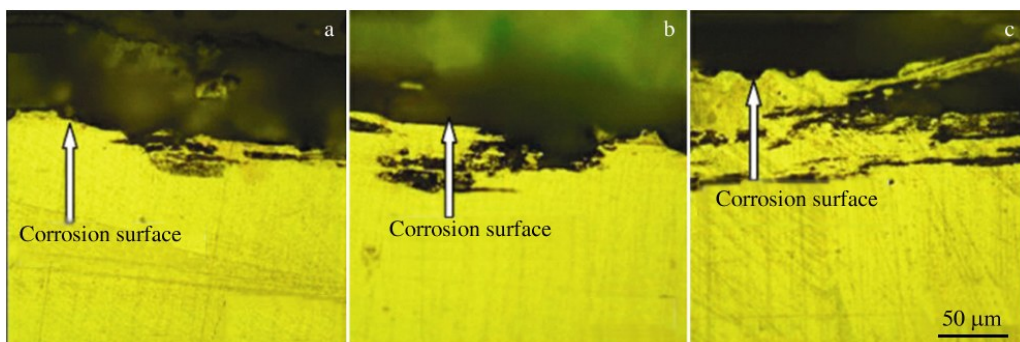

Fig.10 Morphologies of intergranular corrosion of specimens after H-M treatment with different pre-deformations[56]: (a) 3%, (b) 6%, and (c) 8%

al[58] probed the intergranular corrosion and exfoliation corrosion behavior of 2197Al-Li alloy. The main strengthening precipitates of the alloy are δ' phase and T_1 phase when the aging temperature is 175 and 160 °C. In addition, under the heat treatment condition of the same aging time at the aging temperature of 160 °C, the T_1 phase precipitated at the grain boundary of 2197 alloy is more evenly distributed and finer in size. And its corrosion sensitivity is lower in corrosion solution. Liang et al[59] analyzed the effect of aging treatment on the corrosion resistance of deformed Al-3.5Cu-1.5Li-0.22(Sc+Zr) alloy. The intergranular corrosion and exfoliation corrosion sensitivity gradually increases due to the coarsening of T_1 phase and grain boundary precipitate-free zone with the extension of aging time.

In summary, the local corrosion of Al-Cu-Li alloy is closely related to the distribution and size of aging precipitates, especially T_1 phase. The distribution and size of T_1 phase can be controlled by appropriate heat treatment process. The potential difference between intragranular and intergranular phases is reduced and the corrosion resistance of Al-Cu-Li alloy phases is reinforced by the uniform and refined T_1 phase.

2 Corrosion Behavior of Typical Third Generation Al-Cu-Li Alloy in NaCl Solution

2A97Al-Li-Cu alloy is the third generation Al-Li alloy independently developed in China. Compared with typical third generation Al-Cu-Li alloys such as 2060, 2099 and high-strength aluminum alloy 2024, it has superior mechanical properties, admirable welding performance and high damage tolerance[23,30,60–61]. Although scholars have done some research on the corrosion resistance of 2A97 Al-Cu-Li alloy, the corrosion behavior and electrochemical corrosion mechanism of 2A97-T3 and T6 Al-Li alloys in NaCl solution still need to be further explored. The corrosion behavior of 2A97 Al-Li alloy with different heat treatments in NaCl solution is studied by the immersion method and potentiodynamic polarization curve electrochemical method. The 2A97-T3 and T6 Al-Li alloys are the test objects, and the third generation typical 2060-T8 and 2099-T83 Al-Li-Cu alloys and high-strength aluminum alloy 2024-T4 for aviation are the reference objects[62–63].

Fig. 11 exhibits the micromorphologies of the samples soaked in sodium chloride solution of different concentrations for 14 d[62]. The surface of 2A97-T3 and 2A97-T6 specimens demonstrates a network corrosion morphology, which indicates the intergranular corrosion, as shown in Fig. $11a_1$ – $11a_3$ and Fig. $11b_1$ – $11b_3$. With the increase in sodium chloride concentration, the width of corrosion cracks also increases, and the cracks of 2A97-T6 are more than those of 2A97-T3. As shown in Fig. $11c_1$ – $11c_2$, when the corrosion medium is 2wt% and 3.5wt% sodium chloride solution, the corrosion morphologies of 2024-T4 sample are similar to those of 2A97-T3 and 2A97-T6 samples. It is mainly manifested as grain boundary corrosion. When the corrosion medium is 5wt%

sodium chloride solution, the corrosion morphology of 2024-T4 sample is typical layered exfoliation corrosion. As shown in Fig. $11d_1$ – $11d_3$ and Fig. $11e_1$ – $11e_3$, the surface of 2060-T8 and 2099-T83 samples exposes the obvious circular corrosion morphology, and there are clear cracks between the corrosion products.

Fig. 12 is the microscopic morphologies of the samples immersed in sodium chloride solution of different concentrations for 28 d[62]. With the extension of soaking time, the surface corrosion morphology of each sample also presents different degrees of deepening. As shown in Fig. $12a_1$, the massive corrosion products on the surface of 2A97-T3 sample fall off in 2wt% sodium chloride solution. As shown in Fig. $12a_2$, when the corrosion medium is 3.5wt% sodium chloride solution, the typical pitting pits and corrosion rings are observed on the surface of 2A97-T3 samples. As shown in Fig. $12a_3$, when the corrosion medium is 5wt% sodium chloride solution, the irregular block or cellular corrosion products form on the surface of 2A97-T3 sample. As shown in Fig. $12b_1$ – $12b_3$, the corrosion morphologies of 2A97-T6 sample immersed in sodium chloride solution of three concentrations are similar to those of 2A97-T3 sample, but the corrosion morphology of 2A97-T6 sample is more serious than that of 2A97-T3 sample.

As shown in Fig. $12c_1$ – $12c_2$, with the increase in sodium chloride concentration, the pitting pits on the surface of 2024-T4 sample become more obvious. As shown in Fig. $12c_3$, when the corrosion medium is 5wt% sodium chloride solution, the corrosion products on the surface of 2024-T4 sample fall off, and the corrosion morphology is further aggravated. As shown in Fig. $12d_1$ – $12d_3$, as the concentration of sodium chloride solution increases, the corrosion products and pitting pits on the surface of 2060-T8 samples become more obvious. As shown in Fig. $12e_1$ – $12e_3$, the corrosion morphologies of 2099-T83 sample in sodium chloride solution of three concentrations are similar to those of 2060-T8 sample. With the increase in sodium chloride solution concentration, the corrosion pits continue to expand around, and the corrosion products continue to increase and accumulate around the corrosion pits. However, the corrosion pits on the surface of 2099-T83 sample are significantly deeper than those on the surface of 2060-T8 sample.

Fig. 13a displays the potentiodynamic polarization curves of each sample in 3.5wt% NaCl solution. The shapes of the polarization curves are similar and there is no obvious passivation region[63]. Among them, the corrosion current density (I_{corr}) is an important parameter to reflect the corrosion rate of materials. The larger the I_{corr}, the faster the material dissolves and the worse the corrosion resistance. The anodic region of the polarization curve demonstrates the anodic dissolution behavior of the active metal, and the corrosion current density increases exponentially at the beginning of anodic polarization. Fig. 13b exhibits the electrochemical parameter histogram of each sample in 3.5wt% NaCl solution. The corrosion potential (E_{corr}) reflects the difficulty of material corrosion. The larger the E_{corr}, the lower the corrosion
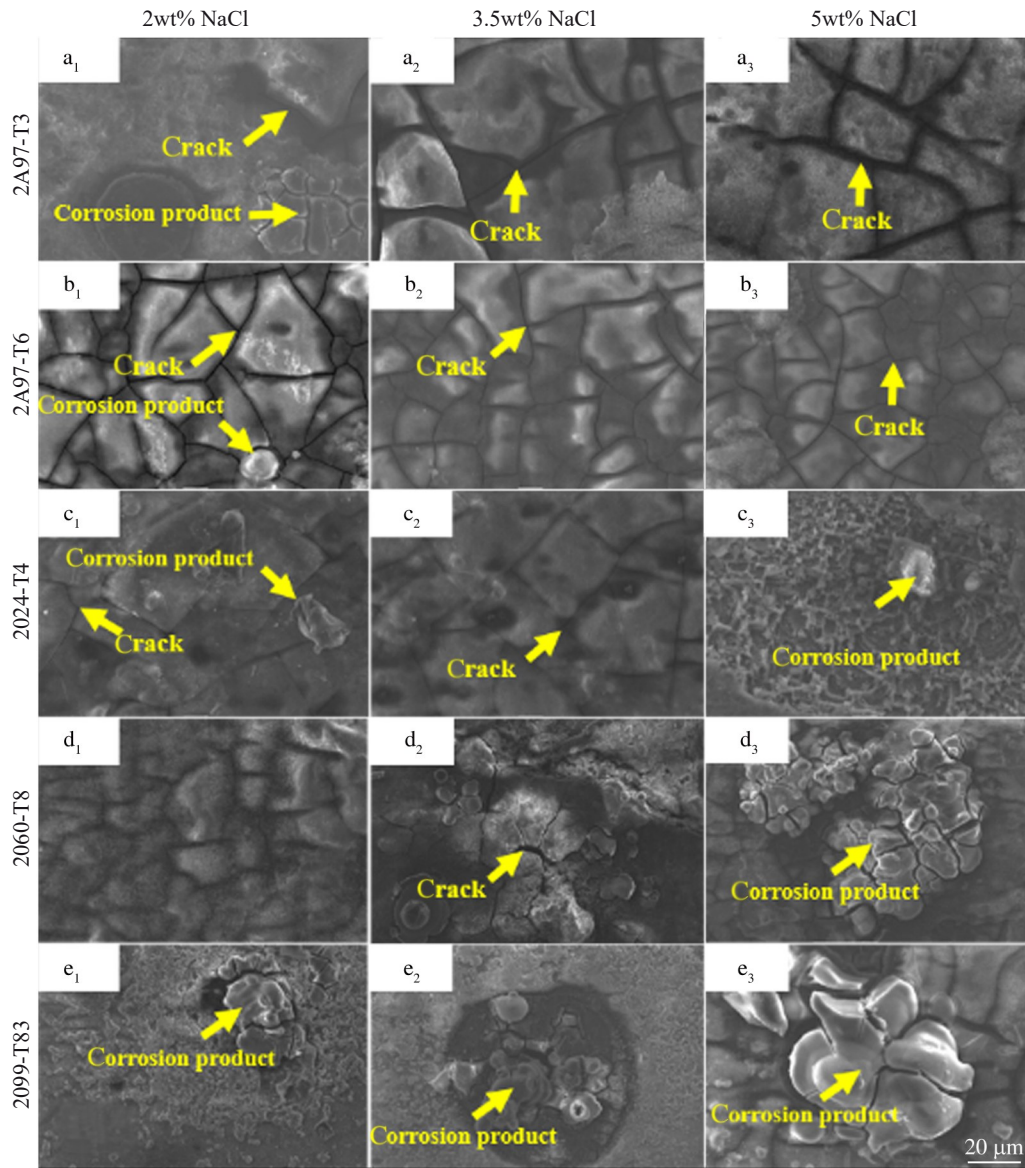
Fig.11 Micromorphologies of samples soaked in sodium chloride solution of different concentrations for 14 d[62]

sensitivity[64–65].

It can be seen from Fig.13b that the order of E_{corr} values of each sample is: 2A97-T3>2024-T4>2A97-T6>2060-T8>2099-T83. The E_{corr} value of 2A97-T3 is the largest, indicating that the corrosion sensitivity of 2A97-T3 Al-Cu-Li alloy is the lowest and the corrosion performance is the best. The E_{corr} of 2024-T4 is between that of 2A97-T3 and 2A97-T6, indicating that the corrosion sensitivity of 2024-T4 is between that of 2A97-T3 and 2A97-T6. The E_{corr} of 2A97-T6 is significantly larger than that of 2060-T8 and 2099-T83 Al-Cu-Li alloys, indicating that the third generation typical 2060-T8 and 2099-T83 alloys are more sensitive to corrosion. They are more prone to corrosion than 2A97-T6 alloy. In addition, the E_{corr} of 2099-T83 is similar to that of 2060-T8, which demonstrates that the corrosion resistance of those two alloys is similar.

Fig.14 presents the surface corrosion and 3D morphology of samples in 3.5wt% NaCl solution. When the concentration of NaCl solution is 3.5wt%, the surface corrosion morphology

area of 2A97-T3 sample is larger, and the pitting pit depth reaches 43.86 μm. The surface corrosion morphology of 2A97-T6 sample is relatively complete, but the pitting pits are increased, and the depth of pitting pits is 49.45 μm. The passivation film of 2024-T4 sample is rapidly broken due to the excessive applied corrosion current. And the pitting corrosion is rapidly initiated, but its corrosion depth is the shallowest among all samples, which is 39.56 μm. The surface corrosion morphology of 2060-T8 sample is more serious than that of 2A97-T6, and the pitting depth is 53.30 μm. The 2099-T83 sample has the largest surface corrosion area and the deepest pitting pit, which is 60.46 μm in pit depth, indicating that the corrosion performance of 2099-T83 Al-Cu-Li alloy is the worst.

The E_{corr} of 2A97 Al-Cu-Li alloy is closely related to the change of aging precipitates. 2A97-T6 is obtained by solid solution (520 °C, 1.5 h) and two-stage aging (200 °C, 6 h and 165 °C, 6h) treatment on the basis of 2A97-T3[66]. After the
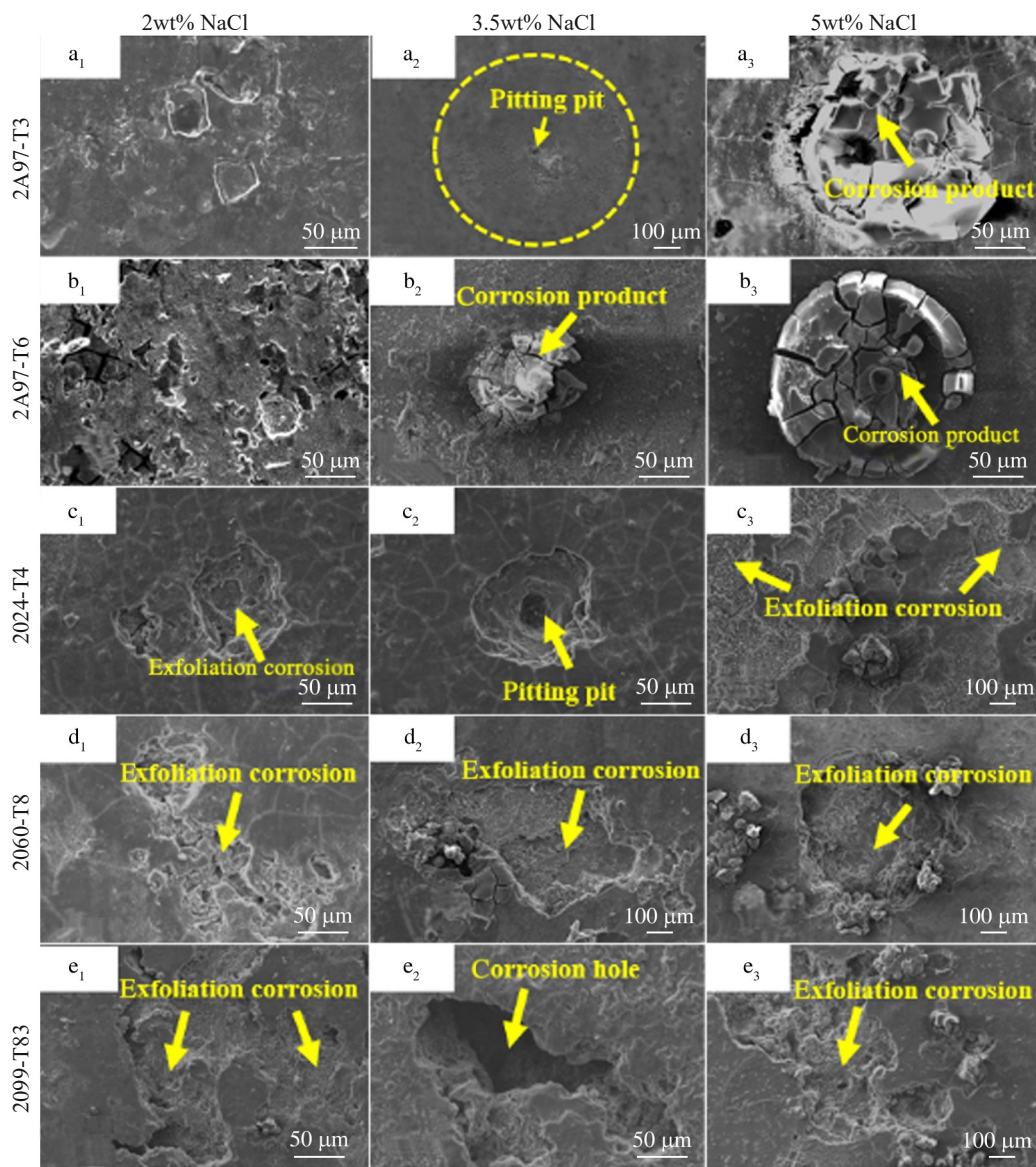
Fig.12   Micromorphologies of samples soaked in sodium chloride solution of different concentrations for 28 d[62]
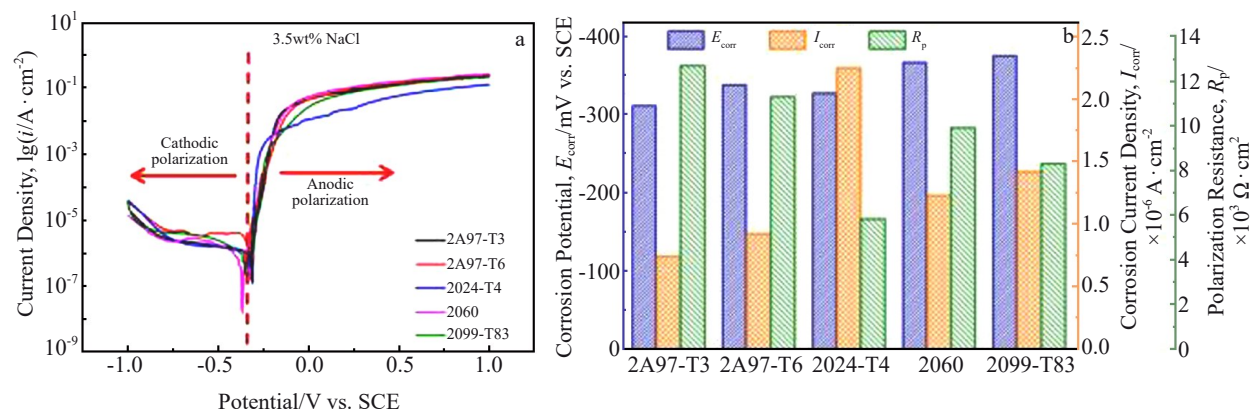

Fig.13   Potentiodynamic polarization curves (a) and electrochemical parameters (b) of the test materials in 3.5wt% NaCl solution[63]

two-stage aging treatment of the 2A97 Al-Cu-Li alloy, lots of T_1 phases are formed near the grain boundary[23,30,55]. In corrosive media, the T_1 phase and the alloy matrix form a

miniature corrosion primary battery. Due to the presence of Li element, the T_1 phase at the grain boundary preferentially dissolves, eventually leading to localized corrosion of the
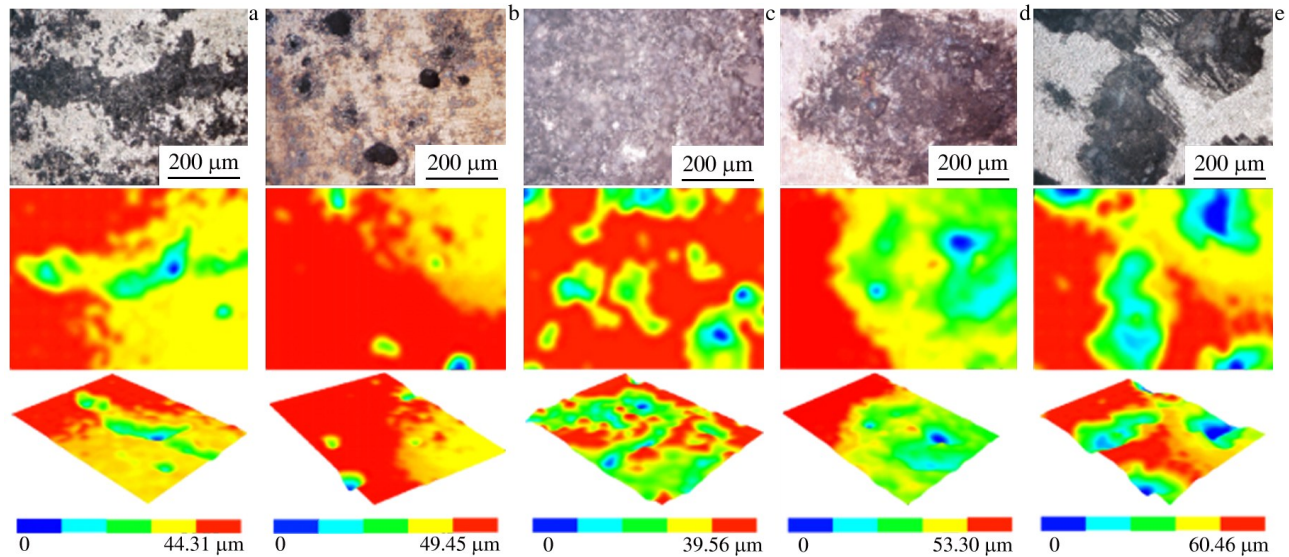
Fig.14　Corrosion surfaces and 3D morphologies of the test materials in 3.5wt% NaCl solution[63]: (a) 2A97-T3, (b) 2A97-T6, (c) 2024-T4, (d) 2060, and (e) 2099-T83

alloy[47,49,67]. Therefore, the corrosion sensitivity of the 2A97-T6 sample is higher than that of the 2A97-T3 alloy.

From the comprehensive analysis of the micromorphologies, potentiodynamic polarization curves, and electrochemical parameter histograms of samples, it can be concluded that the corrosion performance of each sample from strong to weak is: 2A97-T3>2A97-T6>2024-T4>2060-T8>2099-T83.

3　Corrosion Mechanism and Protection of Al-Cu-Li Alloy

3.1　Corrosion mechanism of Al-Cu-Li alloy

When the aircraft is in service in the atmospheric environment, the Al-Cu-Li alloy structure is affected by corrosive Cl^- in the ocean and other humid environment. And there are pitting pits on the alloy surface in a small area. With the extension of the service time, the pitting pit gradually extends to the interior of the alloy, then a local corrosion pit is visible to the naked eye macroscopically, while the rest of the uneroded surface of the alloy is relatively flat.

Fig.15 is the pitting mechanism diagram of aluminum alloy. During the initial period of Al-Cu-Li alloy soaked in NaCl solution, the surface oxide film is in a dynamic equilibrium state of dissolution and re-repair. With the increase in NaCl solution concentration and soaking time, the dynamic balance between the two is broken, and the rate of oxide film rupture on the alloy surface is higher than that of oxide film repair. In the corrosive medium of NaCl solution, the Cl^- ions are preferentially adsorbed on the active sites of the alloy surface than O_2, and Cl^- ions can combine with Al^{3+} on the oxide film to form soluble chlorides, which eventually leads to the formation of pitting pits[68].

A thick liquid film is formed on the surface of Al-Cu-Li alloy during immersion in sodium chloride solution, which hinders the diffusion of O^{2-}. The electrochemical corrosion
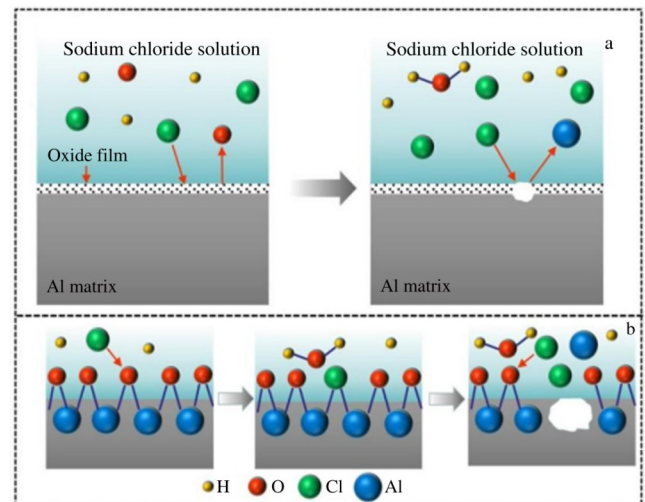

Fig.15　Pitting corrosion (a) and mechanism (b) of oxide film on a sample surface
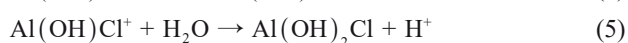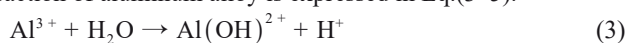
process is mainly a cathodic reaction. Under the action of the corrosive micro-cell, the Al in the anode area firstly dissolves continuously and forms Al^{3+} in the solution and it releases electrons. The electrons migrate to the cathode area. Under the action of the corrosive electrolyte, the oxygen absorption reaction occurs in the cathode area to generate OH^-. Eq. (1) and Eq. (2) are anodic dissolution and cathodic oxygen reduction reactions, respectively.

Anode reaction: $Al - 3e^- \rightarrow Al^{3+}$ 　　　　　　(1)

Cathodic reaction: $O_2 + 2H_2O + 4e^- \rightarrow 4OH^-$ 　　(2)
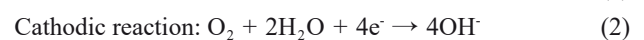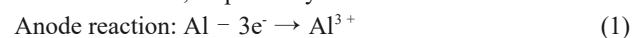
The concentration of Al^{3+} increases with the corrosion reaction in the sodium chloride solution. It is finally hydrolyzed with OH^- ions to form a white product $Al(OH)_3$, which partially meets with the Cl^- ion to form a gray-white product $AlCl_3$. At the same time, the concentration of Cl^- in the

corrosion solution is one of the important influence factors of local corrosion of Al-Cu-Li alloy. With the increase in the concentration of sodium chloride solution, the Cl⁻ ions in the thick liquid film firstly are adsorbed to the active points on the surface of the Al matrix. And then the Cl⁻ ions react with Al^{3+} in the oxide film, resulting in the thinning and local rupture of the oxide film. And finally, the aluminum matrix is exposed to the corrosive medium.

In the corrosive medium containing Cl⁻ ions, the anodic reaction of aluminum alloy is expressed in Eq.(3–5).

$$Al^{3+} + H_2O \rightarrow Al(OH)^{2+} + H^+ \tag{3}$$

$$Al(OH)^{2+} + Cl^- \rightarrow Al(OH)Cl^+ \tag{4}$$

$$Al(OH)Cl^+ + H_2O \rightarrow Al(OH)_2Cl + H^+ \tag{5}$$

In addition, with the increase in the concentration of sodium chloride solution, the concentration of Cl⁻ ions increases, which accelerates the reaction of Eq.(4), resulting in the rapid consumption of the intermediate reaction product $Al(OH)^{2+}$. It eventually leads to the accelerated anodic reaction rate of the Al matrix. At the same time, the insoluble intermediate products can form a compact and protective hydroxide protective film directly near the metal surface, which adheres to the alloy and covers the surface of the Al-Cu-Li alloy to a large extent. It hinders the local corrosion of the alloy. The pitting propagation mechanism of Al-Cu-Li alloy is shown in Fig.16.

The corrosion mechanism of pitting corrosion is that occluded cells are formed in a small area on the metal surface, which leads to the formation and expansion of corrosion pits[69–70].

When the Cl⁻ ions are adsorbed to the oxide film on the surface of aluminum alloy, they react with aluminum ions in the oxide lattice or deposited aluminum hydroxide, resulting

Fig.16   Pitting propagation mechanism of aluminum alloy

in the dissolution of the oxide film. And the Cl⁻ ions directly invade the exposed metal matrix at last.

In some literatures, the corrosion mechanism of Al-Cu-Li alloy is expounded from two aspects of coarse second phase particles and aging precipitates. João et al[24] studied the corrosion behavior of AA2198 Al-Cu-Li alloy at three heat treatment states in NaCl solution. And the corresponding local corrosion mechanism was put forward. The AA2198-T3 alloy matrix undergoes local corrosion, which is around the coarse second phase (Al-Cu-Fe) particles distributed along the deformation direction preferentially, as shown in Fig.17.

As shown in Fig.17b, the coarse second phase particles are displayed on the cross section after the start of the corrosion process. It can be used as the cathode of the corrosion primary cell in the corrosion medium, because the corrosion potential is higher than that of the alloy matrix. As shown in Fig.17c–17d, the alloy matrix around the coarse second phase particles is corroded as an anode for corroding the primary cell, resulting in the formation of grooves in the matrix around the coarse second phase particles. As shown in Fig.17e, the groove depth formed by coarse second phase particles is relatively shallow, indicating that it has little effect on the corrosion resistance of Al-Cu-Li alloy.

As shown in Fig.18a–18b, the grain size of the alloy under the T8 state is significantly different. And the deformation of grain B is the largest, so the T_1 phase density is the highest. Under the state of T851, the stretching before artificial aging is beneficial to the formation of slip bands and the precipitation of T_1 phase, as shown in Fig.19a–19b. Li and Al elements in the T_1 phase preferentially dissolve, which leads to the precipitation of hydrogen, as shown in Fig.18c–18f. The corrosion mechanism of T8 and T851 alloys is the preferential dissolution of T_1 phase in the crystal, which leads to local corrosion of the alloy. However, the corrosion propagation mechanisms of T8 and T851 alloys are different. For the T8 alloy, the grains with large deformation preferentially corrode, and the pre-deformation before aging can form dislocations of high density and uniform distribution inside the grains, which provides the nucleation sites for the T_1 phase. The localized corrosion of T851 alloy is closely related to the selective dissolution of T_1 phase on the slip band, as shown in Fig.19c-19f.

Luo et al[27] researched the pitting corrosion and intergranular corrosion of 2A97-T3 aluminum-lithium alloy. Through video monitoring, it is found that after the sample is immersed in 3.5wt% NaCl solution for a certain period, a certain number of bubbles will be generated in the local area of the sample surface. After the bubbles grow to a certain extent, they are separated from the sample surface. Then the new bubbles will be generated in the same position. The bubbles generated on the surface of the sample are attributed to the hydrogen evolution and oxygen absorption reactions around the coarse second phase particles in the alloy. The chemical reaction formulas are as follows.
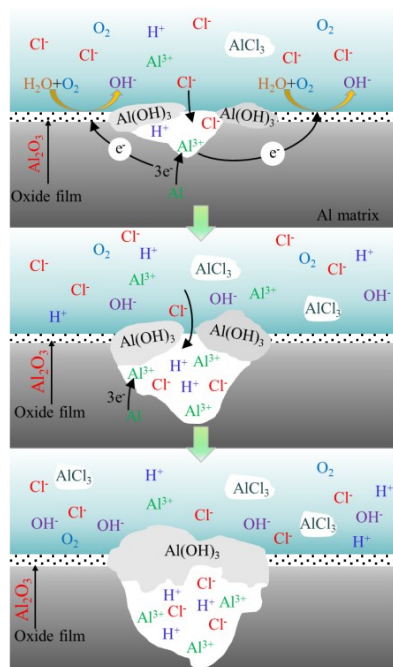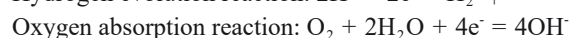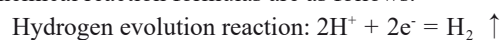
Hydrogen evolution reaction: $2H^+ + 2e^- = H_2 \uparrow$

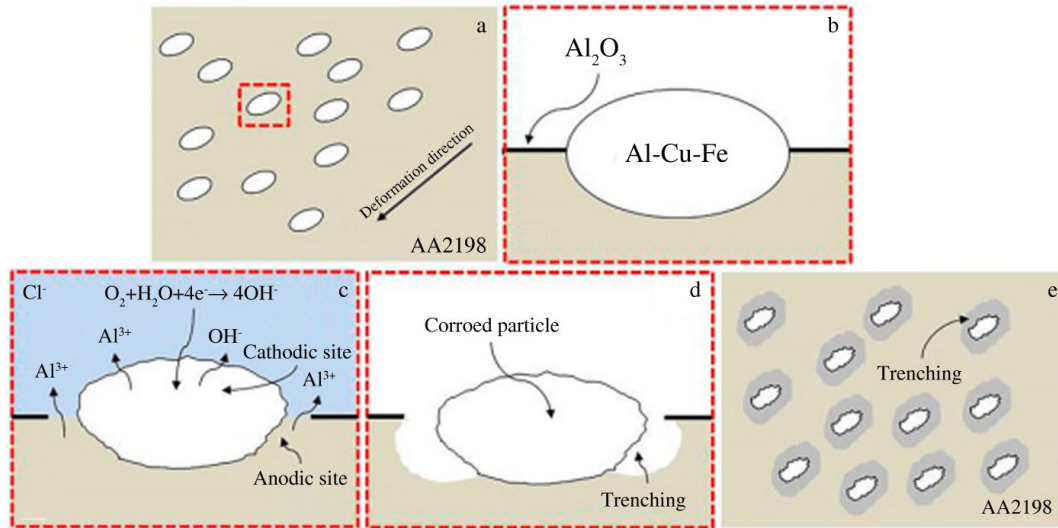Oxygen absorption reaction: $O_2 + 2H_2O + 4e^- = 4OH^-$

Fig.17   Schematic diagrams of the corrosion mechanism associated with second phase particles: (a) polished surface, (b) second phase particles, (c) reaction during immersion in sodium chloride, (d) corrosion characteristics exposed in solution, and (e) corrosion morphology after immersion[24]
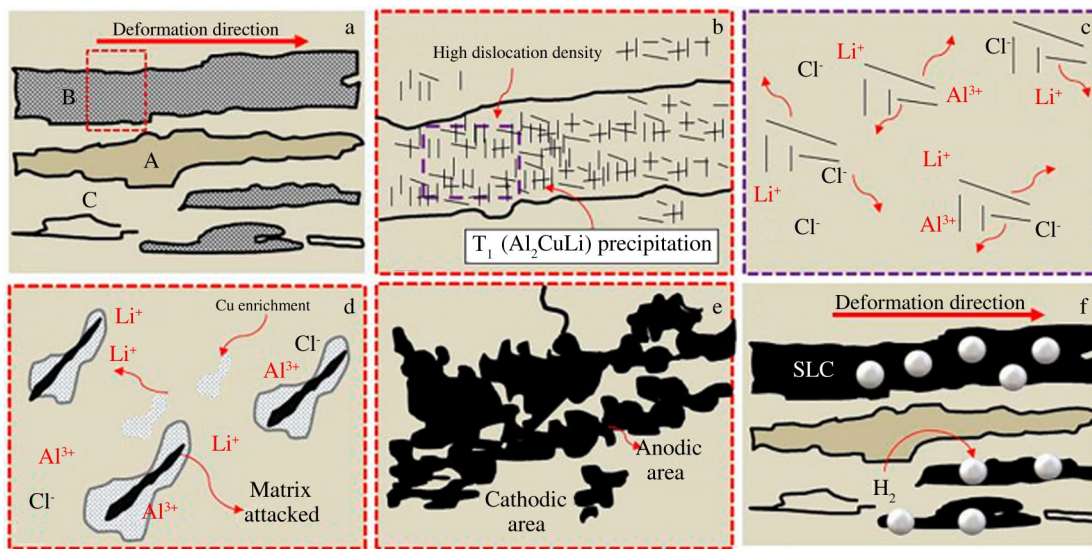

Fig.18   Schematic diagrams of the corrosion mechanism of alloys under T8 conditions: (a) polished surface, (b) grains with T_1 phase of higher density, (c–e) reaction during immersion in sodium chloride, and (f) corrosion characteristics after immersion[24]

The OH^- generated in the above reaction increases the pH value of the corrosive medium. When the pH value of the corrosive environment is greater than 9, the oxide film on the surface of the aluminum alloy cannot exist stably, so the corrosion products on the second phase particles cannot effectively separate the particle surface from the corrosive medium, resulting in the continuous corrosion reaction of the second phase particles with the surrounding alloy matrix.

As shown in Fig.20a–20b, intergranular corrosion is related to the small openings of pitting pits. And it expands along the interior of the alloy, thereby forming a network of corrosion morphologies. The intergranular corrosion starts from the bottom of the corrosion pit. As the corrosion progresses, the degree of pitting corrosion on the surface of the sample

deepens. Then the intergranular corrosion begins to develop from the bottom of the pitting pit. The dissolution of the T_1 phase at the grain boundary provides a large driving force for intergranular corrosion. Corrosion extends along the grain boundary to the interior of the alloy. A network of intergranular corrosion morphology forms completely.

3.2 Protection of aluminum alloys in marine environments

The nano-scale passivated film formed on the surface of Al-Cu-Li alloy is easily broken in the marine environment with high Cl^- content. It causes local corrosion to occur, which can seriously lead to the failure of the marine equipment. To prolong the service life of aircraft and other marine equipment, the corrosion protection is significantly essential.
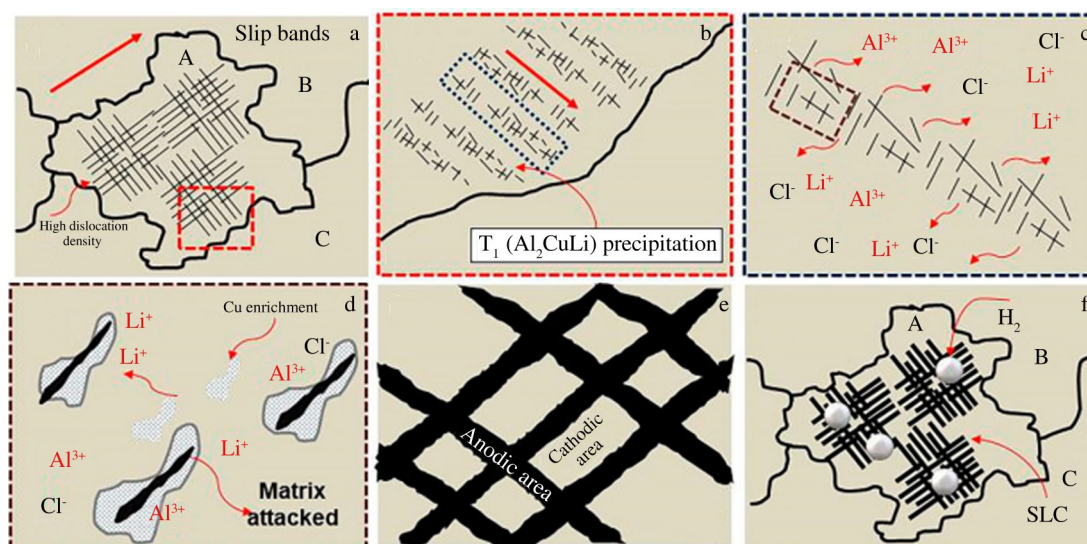
Fig.19   Schematic diagrams of the corrosion mechanism under T851 state: (a) polished surface, (b) reaction of highly dense T_1 phases (c−e) reaction during immersion in sodium chloride, and (f) corrosion characteristics after etching[24]
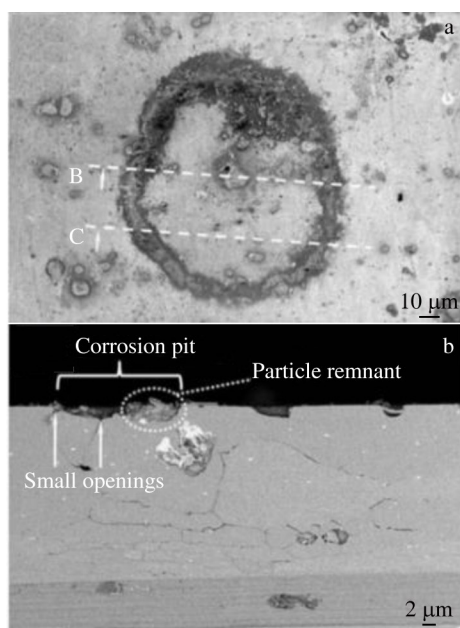

Fig.20   SEM images of corroded area of 2A97-T3 Al-Li alloy after immersion in sodium chloride solution for 2 h: (a) plan and (b) cross section in profile line of direction B[27]

In the marine environment, the common methods of corrosion protection for aluminum alloy are the corrosion inhibitors, the protective coatings, and the electrochemical protection[71–72].

The corrosion inhibitor is a kind of additive that is added to the corrosive medium with appropriate concentration and form, which can prevent or effectively slow down the corrosion of metal materials. At the same time, the addition of corrosion inhibitors does not change the basic properties of metal materials. There are many kinds of corrosion inhibitors, which can be divided into inorganic corrosion inhibitors, organic corrosion inhibitors, and rare earth corrosion inhibitors[73]. There are a few types of inorganic corrosion inhibitors, and they are mainly used in neutral media. Only when the concentration is high, will they show a relatively acceptable metal corrosion effect. Inorganic corrosion inhibitors can produce phosphides, nitrites and chromates. The products have a serious negative impact on the environment, which leads to the eutrophication of water bodies to cause red tides in coastal areas. At present, some inorganic corrosion inhibitors have been gradually replaced by organic corrosion inhibitors[74]. However, the preparation process is complicated, the production cycle is long, and the production cost is high. A green amino acid corrosion inhibitor has been researched with great potential, which is simple in preparation and low in production cost. It has a relatively great anti-corrosion effect on aluminum alloy in an acidic medium[75–76]. Rare earth corrosion inhibitors have broad development prospects in the field of aluminum alloy corrosion protection, due to their advantages of abundant resources, environmental friendliness and low toxicity. However, their film-forming cycle is longer than that of other types of corrosion inhibitors, and the process is also more complicated[77–78]. The synergistic effect of rare earth corrosion inhibitors and other types of corrosion inhibitors is the trend of future research and development.

The protective coating is a coating or film coated on the surface of the material, which can achieve protective functions such as anti-corrosion and anti-oxidation. Therefore, the corrosion resistance and the service life are improved. According to the composition of the protective coating, it can be divided into the metal coating, organic coating and inorganic coating. Metal coating and organic coating are mainly adapted for the surface anti-corrosion of aluminum alloy[79]. The metal coating is generally prepared by laser cladding and spraying[80–81]. Organic coatings are usually produced by coating fluorocarbon, polyurethane, epoxy resin and other anti-corrosive coatings on the surface of aluminum

alloys. Due to the presence of the Cl⁻ ion, the anti-corrosive coating on the surface of the aluminum alloy will be destroyed in the marine environment. And the broken anti-corrosive coating may accelerate the corrosion of the alloy matrix[82]. Therefore, the study of self-healing coatings and their combination with corrosion inhibitors is intensive. However, the preparation of self-healing coatings is complicated and the self-healing ability is poor. It is still in the research and development stage.

Electrochemical protection is one of the commonest metal corrosion protection methods, which can be divided into anodic oxidation and cathodic protection. Anodic oxidation is an electrochemical method to generate a passivation film on the metal surface[83]. The anode passivation film has poor stability in acidic media, which is prone to damage under the stimulation of the external environment. It in turn causes corrosion of the alloy matrix below the passivation film. Therefore, the cathodes are protected by electrochemical method in marine or acidic environments.

Cathodic protection generally refers to the impressed current or the sacrificial anode cathodic protection method. The impressed current cathodic protection method is to apply external current to the protection metal. And the potential is always in the cathode range to ensure that the protection metal is not oxidized. It has the advantages of convenient equipment control, wide application range and long protection period, but the construction of the power supply equipment is difficult[84].

The cathodic protection method of the sacrificial anode is to use the metal with more negative potential to connect with the protective metal to form a corroded primary battery. The added metal with more negative potential is used as the anode, and the protected metal is used as the cathode. The cost of the method is low, but its protection period is short and the anode needs will be replaced regularly[85]. Since the pitting potential of Al-Cu-Li alloys is low, cathodic protection method can be used to improve the corrosion resistance. The combination of cathodic protection and other anti-corrosion methods will be the trend of electrochemical corrosion protection of Al-Cu-Li aluminum alloys[86].

The above corrosion protection technologies have their own limitations. With the development of bionic superhydrophobic process, it provides a new idea for solving the problem in corrosion protection of aluminum alloy. Superhydrophobic surface refers to a solid surface with a static contact angle greater than 150° and a rolling angle (less than 10°)[87]. When the superhydrophobic process is applied to the surface of aluminum alloy, it can effectively prevent the direct contact between the aluminum alloy matrix and the corrosive medium, which can greatly improve the corrosion resistance[88–89].

Zhang et al[90] prepared a superhydrophobic coating on AA1050 aluminum alloy through the anodic oxidation method. And the electrochemical tests were carried out with ordinary hydrophobic coating samples. By comparing the corrosion current density of three materials, it is found that the corrosion resistance of the superhydrophobic coating sample is superior to that of the ordinary hydrophobic coating.

Arunnellaiappan et al[91] made the superhydrophobic coating for AA7075 aluminum alloy by the micro-arc oxidation method, and the electrochemical tests were implemented in 3.5wt% NaCl solution. It is found that the corrosion current density of the superhydrophobic surface is decreased by 6 orders of magnitude, and the impedance is increased by 6 orders of magnitude. It indicates that the corrosion sensitivity of the superhydrophobic sample is low. Zhang et al[92] synthesized a superhydrophobic coating on the surface of pure aluminum by electrochemical deposition. And the electrochemical impedance spectroscopy is actualized in 3.5wt% NaCl solution. The results show that the corrosion rate of the superhydrophobic coating sample is significantly reduced.

The corrosion sensitivity of Al-Cu-Li alloy is greatly improved due to the addition of the lithium element, so it is essential to carry out corrosion protection. Superhydrophobic coatings have been applied to conventional aluminum alloys and have significantly improved the corrosion resistance of materials, which has become the trend of corrosion protection of Al-Cu-Li alloys in the future.

4 Conclusions

1) The effect of coarse second phase particles on the corrosion resistance of typical third generation Al-Cu-Li alloy is significantly different due to different contents of constituent elements. The potential difference between the coarse second phase particles without Li element or with less Li element and the alloy matrix is small. It is used as the cathode of the corrosion galvanic cell in the corrosive medium. And the surrounding alloy matrix is corroded as the anode. The corrosion potential of the coarse second phase particles with higher Li content is more negative than that of the alloy matrix. The Li element preferentially dissolves selectively in the corrosive medium, which makes the coarse second phase particles polarize. The cathode of the corrosion galvanic cell promotes the corrosion of the surrounding alloy matrix.

2) As the main strengthening precipitated phase of Al-Cu-Li alloy, T_1 phase is usually regarded as the anode of the galvanic cell in the corrosive medium of NaCl solution. And the selective dissolution occurs preferentially at the grain boundary. In addition, with the dissolution of Li element, the proportion of Cu element in the T_1 phase increases, resulting in a positive shift of the corrosion potential of the T_1 phase. Then the T_1 phase undergoes a polarity transition and acts as a cathode to corrode the primary battery, which causes the corrosion of the surrounding alloy matrix.

3) Pre-deformation before aging cannot only reduce the potential difference between intragranular and intergranular phases, but also refine the size of T_1 phase in Al-Cu-Li alloy, promoting its uniform precipitation. Thus it reduces the corrosion sensitivity of Al-Cu-Li alloy. At the same time, the size and distribution of T_1 phase can be improved by adjusting the aging temperature and aging time. Then the corrosion resistance of Al-Cu-Li alloy can be improved.

4) The micro-corrosion morphology, corrosion electro-

chemical parameters, surface corrosion morphology and corrosion degree of 2A97-T3, 2024-T4, 2A97-T6, 2060-T8 and 2099-T83 samples are studied by corrosion and electrochemical tests, and the corrosion resistance of each sample from strong to weak is: 2A97-T3>2A97-T6>2024-T4>2060-T8> 2099-T83.

5) The traditional methods of aluminum alloy corrosion protection mainly include corrosion inhibitors, protective coatings, electrochemical protection, etc. All of them have a certain limitation. Superhydrophobic coating has a special structure on the surface of the coating, which makes the alloy have high hydrophobic properties. It can greatly improve the corrosion resistance of aluminum alloy, and has become the trend of corrosion protection of Al-Cu-Li alloy in the future.

References

1 Harsha S, Dasharath. *Materials Today: Proceedings*[J], 2021, 45: 392

2 Wang Y C, Tong G Q, Wu X D *et al. Rare Metal Materials and Engineering*[J], 2021, 50(3): 1069 (in Chinese)

3 Chen R, Wang H M, Sun Z *et al. Materials Letters*[J], 2022, 316: 132 014

4 Wang X, Rong Q, Shi Z S *et al. Materials Science & Engineering A: Structural Materials: Properties, Microstructure and Processing*[J], 2022, 836: 142 723

5 Zhang P, Chen M H. *Journal of Materials Science*[J], 2020, 55: 9828

6 Abd El-Aty A, Xu Y, Guo X *et al. Journal of Research*[J], 2018, 10: 49

7 Xie B X, Huang L, Xu J H *et al. Materials Science and Engineering A*[J], 2022, 832: 142 394

8 Yang Y, He G A, Liu Y *et al. Journal of Materials Science*[J], 2021, 56: 18 368

9 Yang Y, Bi J, Liu H W *et al. Journal of Manufacturing Processes*[J], 2022, 82: 230

10 Dong F, Huang S, Yi Y *et al. Materials Science and Engineering A*[J], 2021, 809: 140 971

11 Zhang Q Y, Zhang C S, Lin J *et al. Materials Science and Engineering A*[J], 2019, 742: 773

12 Rutherford B A, Cisko A R, Allison P G *et al. Journal of Materials Engineering and Performance*[J], 2020, 29: 4928

13 Wright E E, Kaufman M J, Weber G R *et al. Metallurgical and Materials Transactions A*[J], 2020, 51(2): 1012

14 Chen Y, Zheng Z, Cai B *et al. Rare Metal Materials and Engineering*[J], 2011, 40(11): 1926 (in Chinese)

15 Dong F, Huang S, Yi Y *et al. Materials Science and Engineering A*[J], 2022, 834: 142 585

16 Prasad N E, Gokhale A A, Wanhill R J H. *Aluminum Lithium Alloys: Processing, Properties, and Applications*[M]. Butterworth-Heinemann: Elsevier Inc, 2014: 43

17 Chen X X, Zhao G Q, Zhao X T *et al. Journal of Manufacturing Processes*[J], 2020, 59: 326

18 Karthik D, Jiang J C, Hu Y X *et al. Surface and Coatings Technology*[J], 2021, 421: 127 354

19 Su W, Zhu H M. *Corrosion Testing*[J]. 2022, 64(10): 1383

20 Zhao K, Liu J H, Yu Mei *et al. Transactions of Nonferrous Metals Society of China*[J], 2019, 29(9): 1793

21 Chen Y J, Kong F Q, Yang J C *et al. International Journal of Fatigue*[J], 2022, 156: 106 671

22 Liew Y H, Ornek C, Pan J S *et al. Electrochimica Acta*[J], 2021, 392: 139 005

23 Zhang X X, Lv Y, Zhou X R *et al. Journal of Alloys and Compounds*[J], 2022, 898: 162 872

24 João V S A, Aline F S B, Donatus U *et al. Corrosion Engineering Science and Technology*[J], 2019, 54(7): 575

25 Liu D Y, Ma Y L, Li J F *et al. Materials Characterization*[J], 2020, 167: 110 528

26 Niu J T, Liu Z Q, Qiao Y *et al. Materials and Corrosion*[J], 2022, 73(2): 171

27 Luo C, Albu S P, Zhou X *et al. Journal of Alloys and Compounds*[J], 2016, 658(2): 62

28 Ma Y, Zhou X, Huang W *et al. Materials Chemistry & Physics*[J], 2015, 161: 201

29 Zhang Z Q, Wang Y L, Li L F. *Advances in Materials Science and Engineering*[J], 2022, 1

30 Zhang X, Zhou X, Hashimoto T *et al. Corrosion Science*[J], 2017, 116: 14

31 Kertz J E, Gouma P I, Buchheit R G. *Metallurgical and Materials Transactions A*[J], 2001, 32(10): 2561

32 Buchheit R G, Moran J P, Stoner G E. *Corrosion*[J], 1990, 46: 610

33 Mao Y, Gokhale A M, Harris J. *Computational Materials Science*[J], 2006, 37(4): 543

34 Ma Y L, Zhou X R, Liao Y *et al. Corrosion Science*[J], 2016, 107(6): 41

35 Ma Y, Zhou X, Thompson G E *et al. Materials Chemistry Physics*[J], 2011, 126(1–2): 46

36 Vicente A P, Baptiste G, Frederic D G *et al. Acta Materialia*[J], 2014, 66: 199

37 Chen B B, Guo M F, Zheng J X *et al. Advanced Engineering Materials*[J], 2016, 18(7): 1225

38 Decreus B, Deschamps A, Geuser F D *et al. Acta Materialia*[J], 2013, 61(6): 2207

39 Germer J J, Zein N N, Metwally M A *et al. Acta Materialia*[J], 2013, 61(11): 4010

40 Wang S C, Starink M J. *International Materials Reviews*[J], 2005, 50(4): 193

41 Balbo A, Frigani A, Grassi V *et al. Materials & Corrosion*[J], 2015, 66(8): 796

42 Ma Y, Zhou X, Thompson G E *et al. Corrosion Science*[J], 2011, 53(12): 4141

43 Lin Y, Zheng Z Q, Li S C *et al. Rare Metal Materials and Engineering*[J], 2014, 43(6): 1467 (in Chinese)

44 Dolega, Adamczykcies'lak B, Mizera J *et al. Journal of Materials Science*[J], 2012, 47(7): 3026

45 Huang J L, Li J F, Liu D Y *et al. Corrosion Science*[J], 2018, 139: 215

46 Li J F, Zheng Z, Na J *et al. Materials Chemistry and Physics*[J], 2005, 91(2–3): 325

47 Li J F, Li C X, Peng Z W *et al. Journal of Alloys and Compounds*[J], 2008, 460: 688

48 Rinker J G, Marek M, Sanders Jr T H. *Materials Science and Engineering*[J], 1984, 64: 203

49 Buchheit R G, Moran J P, Stoner G E. *Corrosion*[J], 1994, 50: 120

50 Ghosh K S, Das K, Chatterjee V K. *Materials Science and Technology*[J], 2004, 20(7): 825

51 Gable B M, Zhu A W, Csontos A A *et al. Journal of Light Metals*[J], 2001, 1(1): 1

52 Cassada W A, Shiflet G J, Starke E A. *Metallurgical and Materials Transactions A*[J], 1991, 22(2): 299

53 Ringer S P, Muddle B C, Polmear I J. *Metallurgical and Materials Transactions A*[J], 1995, 26(7): 1659

54 Tsivoulas D, Prangnell P B. *Metallurgical and Materials Transactions A*[J], 2014, 45(3): 1338

55 Li H Y, Tang Y, Zeng Z D *et al. Chinese Journal of Nonferrous Metal*[J], 2008, 18(4): 778

56 Xu Y, Wang X J, Yan Z T *et al. Chinese Journal of Aeronautics*[J], 2011, 24: 681

57 Yuan Z S, Lu Z, Xie Y H *et al. Rare Metal Materials and Engineering*[J], 2007, 36(3):493 (in Chinese)

58 Jiang N, Li J F, Zheng Z Q *et al. Transactions of Nonferrous Metals Society of China*[J], 2005, 1(1): 23

59 Liang W, Pan Q, He Y *et al. Rare Metals*[J], 2008, 27(2): 146

60 Zhang X X, Liu B, Zhou X R *et al. Corrosion Science*[J], 2018, 135: 177

61 Lei X W, Nuam V L, Bai Y *et al. Journal of Alloys and Compounds*[J], 2021, 855: 157 519

62 Wang Z Y, Zhang P, Zhao X S *et al. Coatings*[J], 2022, 12(12): 1899

63 Zhang P, Zhao X S, Rao S X. *Rare Metal Materials and Engineering*[J], 2023, 52(5): 1573

64 Osório W R, Freitas E S, Garcia A. *Electrochimica Acta*[J], 2013, 102: 436

65 Bononi M, Conte M, Giovanardi R *et al. Surface and Coatings Technology*[J], 2017, 325: 627

66 Zhang P, Chen M H, Chen W *et al. Microscopy Research and Technique*[J], 2021, 84(2): 358

67 Li J F, Zheng Z Q, Li S C *et al. Corrosion Science*[J], 2007, 49(6): 2436

68 Szklarska-Smialowska Z. *Corrosion Science*[J], 1999, 41(9): 1743

69 Muller I L, Galvele J R. *Corrosion Science*[J], 1977, 17(3): 179

70 Zhang X X, Zhou X R, Hashimoto T *et al. Materials Characterization*[J], 2017, 130: 230

71 Silva C M, Blawert C, Scharnagl N *et al. Materials*[J], 2022, 15(4): 1301

72 Liu Y, Cao H J, Chen S G *et al. The Journal of Physical Chemistry C*[J], 2015, 119(45): 25 449

73 Mohammadi I, Shahrabi T, Mahdavian M *et al. Journal of Molecular Liquids*[J], 2020, 307: 112 965

74 Ji J T, Dong Y H, Wen J J *et al. Ordnance Material Science and Engineering*[J], 2023, 46(1): 127 (in Chinese)

75 Zhang O H, Jiang Z N, Li Y Y *et al. Chemical Engineering Journal*[J], 2022, 437: 135 439

76 Sorkhabi A H, Ghasemi Z, Seifzadeh D. *Applied Surface Science*[J], 2005, 249: 408

77 Fan X Y, Chen B S, Ding J H *et al. Contemporary Chemical Industry*[J], 2018, 47(1): 136 (in Chinese)

78 Gu B S, Gong L, Yang P Y. *Rare Metal Materials and Engineering*[J], 2014, 43(2): 429 (in Chinese)

79 Hou Y, Tian Y, Zhao Z P *et al. Surface Technology*[J], 2022, 51(5): 1 (in Chinese)

80 Naimi A, Yousfi H, Trari M. *Protection of Metals and Physical Chemistry of Surfaces*[J], 2012, 48(5): 557

81 Zeng X P, Wang Q L, Ma Y X *et al. Powder Metallurgy Industry*[J], 2022, 32(5):74 (in Chinese)

82 Fu C W, Wang G C. *Shanxi Chemical Industry*[J], 2021, 41(3): 20 (in Chinese)

83 Wu H Q, Hebert K R. *Electrochimica Acta*[J], 2002, 47(9): 1373

84 Kainuma S, Yang M Y, Ishihara S *et al. Construction and Building Materials*[J], 2019, 224: 880

85 Dinh T V, Sun W W, Yue Y *et al. Corrosion Science*[J], 2018, 145: 67

86 Hartt W H, Edward J L, Keith E L. *Corrosion 2001*[C]. Texas: NACE International, 2001: 11

87 Shirtcliffe N J, Mchale G, Atherton S *et al. Advances in Colloid and Interface Science*[J], 2010, 161(1): 124

88 Li X W, Wang H X, Shi T *et al. Rare Metal Materials and Engineering*[J], 2022, 51(1): 6

89 Zhang C W, Li X W, Shi Tian *et al. Rare Metal Materials and Engineering*[J], 2018, 47(10): 2980

90 Zhang H F, Yin L, Shi S Y *et al. Microelectronic Engineering*[J], 2015, 141(15): 238

91 Arunnellaiappan T, Arun S, Hariprasad S *et al. Ceramics International*[J], 2018, 44(1): 874

92 Zhang B B, Xu W C, Zhu O J *et al. Journal of Colloid Interface Science*[J], 2018, 532: 201

Al-Cu-Li合金在盐溶液中的腐蚀行为以及腐蚀机理研究进展

张　鹏[1,2,3]，包　磊[1]，饶思贤[1]，吴进军[2]，李永兵[3]，熊成悦[3]，孙朝阳[4]

(1. 安徽工业大学 机械工程学院，安徽 马鞍山 243032)

(2. 中国机械科学研究总院集团有限公司，北京 100044)

(3. 北京机科国创轻量化科学研究院有限公司 先进成形技术与装备国家重点实验室，北京 100083)

(4. 北京科技大学 机械工程学院，北京 100083)

摘　要：Al-Cu-Li合金是航天航空工业中重要的轻质结构材料，已成为国产大飞机结构件的关键材料之一。飞行器在海洋等潮湿环境服役时，易受到具有腐蚀性的卤化物阴离子的侵蚀，尤其是在Cl⁻离子侵蚀作用下，Al-Cu-Li合金构件表面易出现点蚀、晶间腐蚀和剥落腐蚀现象。Al-Cu-Li合金的局部腐蚀主要归因于合金相与合金基体间存在电势差，进而导致在腐蚀介质中形成微型腐蚀原电池。综述了Al-Cu-Li合金在NaCl溶液中的腐蚀行为以及热处理工艺对合金耐腐蚀性能的影响，重点分析了粗大第二相颗粒和时效析出相对Al-Cu-Li合金腐蚀性能的影响，研究了典型第3代Al-Cu-Li（2A97-T3、2A97-T6、2060-T8和2099-T83）合金以及航空用常规高强铝合金2024-T4在3种不同浓度NaCl溶液中的侵蚀行为以及在质量分数3.5%NaCl溶液中的电化学行为。综合分析各试样的微观腐蚀形貌、腐蚀电化学参数以及腐蚀程度，最终得出各试样的耐腐蚀性能由强至弱为：2A97-T3>2A97-T6>2024-T4>2060-T8>2099-T83。最后揭示了Al-Cu-Li合金在腐蚀介质中的腐蚀机理，总结了在海洋环境下铝合金的防腐措施。本文为后续Al-Cu-Li合金防腐性能的发展和飞机耐腐蚀性能的提升提供了参考。

关键词：Al-Cu-Li合金；合金相；局部腐蚀；腐蚀机理；腐蚀防护